Ab initio calculation of lattice dynamics in BeO

2008 J. Phys.: Condens. Matter 20 395201

(http://iopscience.iop.org/0953-8984/20/39/395201)

J. Phys.: Condens. Matter **20** (2008) 395201 (7pp) doi:10.1088/0953-8984/20/39/395201

Ab initio calculation of lattice dynamics in BeO

Munima B Sahariah[1] **and Subhradip Ghosh**[2]

[1] Institute of Advanced Study in Science and Technology, Guwahati-781035, India
[2] Indian Institute of Technology Guwahati, Guwahati-781039, India

E-mail: munimab@gmail.com and munima@alumni.iitg.ernet.in

Received 27 May 2008, in final form 10 July 2008
Published 1 September 2008
Online at stacks.iop.org/JPhysCM/20/395201

Abstract

Ground state lattice vibrational properties of wurtzite–BeO are reported using an *ab initio* plane-wave pseudopotential method. The *ab initio* results for the phonon dispersion relations are in good agreement with the available experimental data. The only discrepancy observed between experiment and present data for the longitudinal optic frequency at the centre of the Brillouin zone for a displacement along the symmetry axis is expected to be due to the indirect measurement of that mode in the experiment. The dielectric constant, the Born effective charges and the elastic constants for the compound are computed from the lattice dynamics. All of them agree well with the experimental results. The elastic constants calculated using the phonon spectra agree reasonably well with the results from other first-principles calculations. The good agreement of the quantities calculated, with the experimental results pave the way for future studies on the contribution of lattice vibrations to the pressure-induced phase transition in this compound. We try to understand the features of the phonon spectra from the component-projected phonon densities of states and by analysing the contributions of each atom type towards each normal mode. We find that the phonon spectra of BeO contains features common to some of the members with the same crystal structure as well as to some of the members in the same alkaline earth oxide group.

(Some figures in this article are in colour only in the electronic version)

1. Introduction

The presence of oxygen in different compounds has always attracted the attention of the scientific community due to the significantly high chemical reactivity of the oxygen with its surroundings. Alkaline earth oxides are an important class of oxides as they are fundamental materials for industrial research and are comparatively simple in their structure. They act as the prototype to other ionic oxides and are widely used as precursors for processing a large variety of materials in the chemical industry. BeO, one member of this class, which is a low-Z oxide and the lightest II–VI compound, is of particular importance because of its high thermal and low electrical conductivity. Unlike the other members of its class (MgO, CaO, SrO and BaO) all having cubic symmetry, BeO has hexagonal symmetry. At ambient pressure and temperature BeO crystallizes in the wurtzite structure and belongs to the space group C_{6V}^4 ($P6_3mc$) with two formula units per unit cell and with all atoms occupying C_{3v} sites [1]. The structure is illustrated in figure 1.

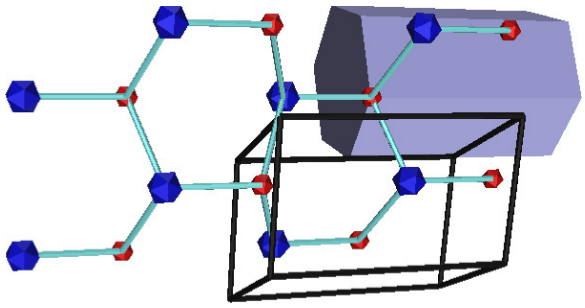

Figure 1. The perspective view of a BeO crystal illustrated along [100] direction. The larger balls are for oxygen, smaller ones are for beryllium. The unit cell and the Wigner-Seitz cell are also shown in the figure.

There is a lot of controversy regarding the temperature and pressure where BeO undergoes structural transformations [2–6]. In all these calculations, the role of vibrational contributions towards the phase transformation has been

neglected altogether, whereas it is known to play a significant role. The contribution towards the entropy from the vibrational part can lower the free energy, stabilizing one phase over the other at a given temperature and pressure. Therefore, the controversy related to the correct pressure and temperature ranges for the structural transformation and the underlying mechanism can be resolved by explicit consideration of vibrational contributions. Reliable and accurate information on the lattice dynamics or the vibrational properties can be obtained from *ab initio* electronic structure calculations. Thermodynamic properties like specific heat, heat transport etc are closely related to the atomic vibrations in the crystal and can be derived from the dispersion relations. The phonon dispersion relation also helps in understanding the phonon density of states, which in turn can be related to the reaction kinetics of a system. Even though wurtzite crystals exhibit one of the simplest structures, and therefore form an important class of materials, very few attempts have been made to completely understand the full phonon dispersion relation of BeO in the ground state. No *ab initio* calculation has yet been done to study the ground state lattice dynamics of this material. Several theoretical groups [7, 8] have made only preliminary calculations, either from lattice potential or from the valence force field, to obtain the dispersion relation in BeO. The picture is also not encouraging from the experimental point of view. The first set of neutron scattering data was given by Brugger *et al* [9] for a few modes of the spectra along two symmetry directions. However, later it was found that the low lying optical branches reported in this work are actually the result of some multiphonon process [8]. The later work [8] reported some new branches along the same symmetry directions and also mapped the whole spectra with these data and the existing Raman scattering data for optical frequencies at Γ from Loh [10].

As a preparatory work towards studying the lattice dynamics of BeO under pressure and temperature, here we present the vibrational properties of BeO in its ground state using the *ab initio* density functional perturbation theory. The paper is organized as follows: sections 2 and 3 describe the theoretical background and computational details. Section 4.1 describes the results of USPP generation for the Be atom and in section 4.2 we present the equilibrium lattice parameters from the *ab initio* calculations. Section 4.3 shows the complete phonon spectra along with the partial phonon density of states. Here we also present a mode by mode analysis of the contribution from both the atom types to the phonon frequencies along several symmetry directions. Here we also compare our *ab initio* data with the available experimental data. In section 4.4 LO–TO splitting of the optical vibrational modes associated with the macroscopic electric field are discussed. Finally we compute the elastic constants of wurtzite–BeO to test the accuracy of interatomic forces calculated by the present method in section 4.5. Conclusions and future directions are provided in section 5.

2. Theoretical background

The electronic structure and lattice dynamics of beryllium oxide are calculated using density functional perturbation theory (DFPT) [11, 12]. DFPT is a density functional theory [13–15] based on a linear response method capable of computing the electronic structure as well as responses to phonon excitations at any arbitrary wavevector. It is a very flexible and powerful technique for calculating the lattice vibrational properties which depend on the system response to perturbations in the form of displacements. The lattice distortion corresponding to a given phonon excitation can be considered as a static perturbation acting on the electrons of the crystal. In DFPT, the linear density response of the system to this perturbation is calculated self-consistently via the solution of a set of equations which involve only quantities related to the unperturbed crystal with the atoms in their undisplaced configuration. Unlike the conventional frozen phonon method, DFPT has no restriction to high symmetry points and phonon frequencies can be calculated at an arbitrary wavelength. In ionic materials, the displacements of charges creates dipoles which produce a macroscopic electric field in the limit of zero wavevector. These are responsible for a splitting of the frequencies of the optical vibrational modes parallel and perpendicular to the electric field, more commonly known as the LO–TO splitting. The linear response method provides a natural way of dealing with the LO–TO splitting in these materials.

One efficient way to test the accuracy of the interatomic forces and the phonons is to compute the elastic constants of the system. Elastic constants can be obtained from the slopes of the acoustic phonon branches in the long wavelength limit. All the six different elastic coefficients typical of hexagonal symmetry were calculated, out of which only five were independent. This requires acoustic phonon branches propagating in two different directions, one along the symmetry axis and the other perpendicular to it.

DFPT has been implemented in the framework of plane-wave pseudopotential theory and linearized Muffin-tin orbital theory. Here, we have used the former framework which is easily implementable and more tractable.

3. Computational details

First-principles Quantum-Espresso code [16] which implements DFPT within a plane-wave-pseudopotential framework has been used to calculate the lattice dynamics of BeO. Ultrasoft pseudopotentials [17, 18] generated using Vanderbilt's scheme [19] were used. Non-linear core corrections [20] were implemented in the generation of the pseudopotential. The Be pseudopotential was generated by us and the oxygen pseudopotential was used from the Quantum-Espresso database [21]. PW-91 [22] functionals were used for the exchange–correlation part of the potential. The kinetic energy cutoff was taken to be 45 Ryd. The Brillouin zone integration was performed over a Monkhorst–Pack [23] $8 \times 8 \times 5$ mesh. These parameters converged the phonon frequencies to within 1%. Only at the Γ and A point, the frequencies converged at a higher k-mesh of $14 \times 14 \times 9$. The dynamical matrices were calculated on a mesh of $6 \times 6 \times 4$ q-points in the irreducible Brillouin zone, which resulted in 47 q-points. Real-space force constants were obtained by Fourier transform. The dispersion curves

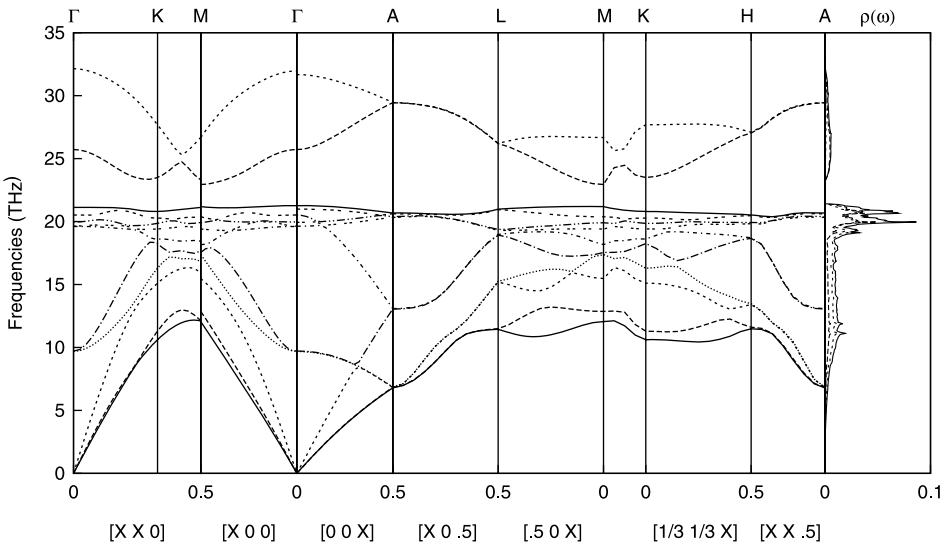

Figure 2. Phonon dispersion relations along various symmetry directions in the first Brillouin zone for wurtzite–BeO. The rightmost plot is for the phonon density of states.

Table 1. Valence s and p levels, the total energies for ground and excited states for AE and pseudopotential case. Units are in Ryd.

State		AE	Pseudo	Diff.
s^2p^0 (ref.)	s	0.414 379	0.414 379	0.0
	p	0.150 829	0.150 829	0.0
s^1p^1	s	0.455 359	0.454 933	0.000 426
	p	0.188 283	0.188 283	0.000 113
s^1p^0	s	1.008 715	1.008 455	0.000 260
	p	0.720 187	0.720 477	0.000 290

were calculated by diagonalizing the dynamical matrix and the densities of states were calculated by Eyvaz Esaev's code.

4. Results and discussions

4.1. Ultrasoft pseudopotential for Be

The Ultrasoft pseudopotential for Be was generated using Vanderbilt's scheme. The pseudopotential was generated in the ground $1s^22s^2$ configuration. Both s and p orbitals were treated as valence ones. The cutoff radius r_c for both the orbitals were set at 1.5 au. To improve the transferability of the pseudopotential, we also included contributions from excited states. In table 1 we show the valence s and p levels for various states with their total energies for all-electron and pseudopotential cases. The minimum difference between all-electron and pseudopotential eigenvalues was less than 1 mRyd which suggests the reliability of the pseudopotential.

4.2. Ground state properties

For the wurtzite structure, the ground state is obtained by minimizing the total energy with respect to the lattice parameters a, c/a and internal parameter u. The equilibrium values for all these parameters are listed in table 2. Comparison

Table 2. Equilibrium lattice parameters for BeO in au.

	a	c/a	u
Theor.	5.10	1.637	0.377
Exptl.	5.12	1.620	0.378

with the experimental values [24, 25] suggest that the agreement is pretty good (maximum deviation is 1% for c/a).

4.3. Phonon dispersion

Wurtzite-BeO has two formula units per unit cell. Therefore, there are twelve phonon modes for a given wavevector. According to the group theory analysis at the Γ-point, the optical and acoustic phonons belong to the following irreducible representations [26].

$$\Gamma_{\text{opt}} = \mathrm{A}_1(Z) + 2\mathrm{B} + 2\mathrm{E}_1(X, Y) + 2\mathrm{E}_2$$

$$\Gamma_{\text{ac}} = \mathrm{A}_1(Z) + \mathrm{E}_1(X, Y).$$

Here optical phonons belonging to A_1, E_1 and E_2 modes are Raman active. Out of these A_1 and E_1 modes are also infrared active. Phonons belonging to B modes are silent. A_1 and E_1 mode phonons are the polar phonons and split into LO and TO modes.

The phonon dispersion relations of BeO along several symmetry directions are calculated and the results are shown in figure 2. Different linestyles have been used to show different representations. The rightmost plot of the figure shows the one-phonon DOS and the projected DOS corresponding to beryllium and oxygen displacements. In figure 3 we show the phonon density of state plots separately. For this particular crystal structure, the Γ and M points are symmetry critical points [27]. The slight discontinuity of some phonon modes at Γ and M point is attributed to the difference in LO–TO splitting when there is a change in direction of the phonon propagation.

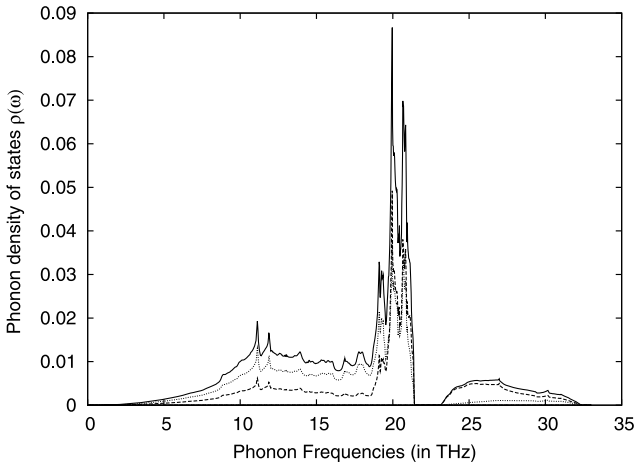

Figure 3. The plots for phonon density of states. The solid curves represent the total DOS, whereas the - - - - and · · · · · · curves display the projected DOS corresponding to beryllium and oxygen displacements, respectively.

This does not occur at other symmetry points as can be seen from the figure. We list interpolated phonon frequencies at several high symmetry points in table 3.

The density of states plot in figure 3 shows that the phonon states are densely populated in the region around 18–21 THz. This behaviour can also be seen in CaO [28]. The fact that a gap appears in the phonon dispersion is shared by other materials like ZnO, GaN etc [29, 27] having the same structure and the same space group. However the other members of the alkaline earth oxides group (MgO, CaO, SrO) having a rocksalt phase do not show such a gap in their dispersion relation [28]. The gap in the phonon DOS basically separates beryllium dominated vibrations from mixed oxygen and beryllium vibrations.

Experimental measurements of phonon dispersions are available for a few modes and along two directions only [9, 8]. In figure 4 we plot the dispersion relation along [01$\bar{1}$0] and [0001] directions to explicitly show the agreement with the experimental data from neutron inelastic scattering available along these directions [8]. We can see from the figure that the neutron scattering data has good agreement with our *ab initio* ones. In the figure we also show the first order Raman scattering data from Arguello *et al* [30] in the [01$\bar{1}$0] plot and that from Loh [10] in the [0001] plot for the optic modes at the centre of the Brillouin zone. The discrepancy between the experimental and theoretical phonon frequencies at Γ for some higher modes is discussed in section 4.4.

A complete analysis of the contributions from beryllium and oxygen sublattices to all the 12 modes of the phonon spectra are shown in figure 5 by plotting the squared vibrational amplitudes along various branches. We can see from the figure that at higher modes (above the gap) there is a complete splitting of contributions amongst the two sublattices. The average contribution from the beryllium sublattice is about 85%. This is as expected because beryllium is lighter than oxygen. At lower modes it is the oxygen which contributes more. For modes which lie in between, there are mixed contributions. For all three acoustic modes both oxygen and beryllium contribute equally (50% each) at the centre of the Brillouin zone (Γ point).

Table 3. Phonon frequencies at some high symmetry points. Frequencies are in units of THz.

Symmetry point	Freq.	Symmetry point	Freq.	Symmetry point	Freq.
	0.00		10.61		12.09
	0.00		11.29		12.14
	0.00		15.10		15.93
	9.68		16.29		16.85
	9.71		18.25		17.66
Γ	19.61	K	18.61	M	18.44
	19.63		19.41		19.47
	19.97		19.86		19.92
	20.52		20.28		20.30
	21.12		20.80		21.12
	25.72		23.50		23.30
	32.14		27.69		26.68
	6.79		11.48		11.44
	6.82		11.61		11.49
	6.83		13.42		15.19
	6.85		13.48		15.25
	13.05		18.66		18.92
A	13.09	H	18.70	L	18.97
	20.33		19.83		19.30
	20.39		19.92		19.37
	20.61		20.47		20.94
	20.67		20.53		20.99
	29.43		27.04		26.18
	29.45		27.10		26.21

4.4. LO–TO splitting at the centre of the Brillouin zone (Γ-point) in BeO

Figure 6 shows the atomic displacement patterns for both E_1 and A_1 branches split into LO and TO modes. For the E_1 branch, atoms in the same sublattice vibrate in the same direction while each sublattice vibrates in a direction opposite to the other. The vibrations are in planes perpendicular to the symmetry axis. For the A_1 type of vibrations, atoms vibrate along the symmetry axis with each atom of a sublattice vibrating opposite to each other. For each mode we show the corresponding frequencies and compare them with the Raman and infrared scattering data.

The results show that except for the A_{1L} mode, where the *ab initio* value differs by about 25% from the experimental one, all the other three modes have very good agreement with the experimental ones (within 3%). This large difference in the frequencies of the A_{1L} phonon could be due to the indirect observation of this phonon in the experiment. The direct observation of the A_1 longitudinal phonon requires a 45° cut crystal and the samples used in the experiments were not large enough for that. So, in that case, the A_1 longitudinal peak was observed [10] from the unanalysed right angle Raman spectrum and in another case [30] from back scattering and forward scattering diagrams. On the other hand our *ab initio* value for the A_{1L} phonon mode (25.72 THz) is close to the one estimated from the beryllium oxide dispersion relation worked out by Ostheller (23.09 THz) [8].

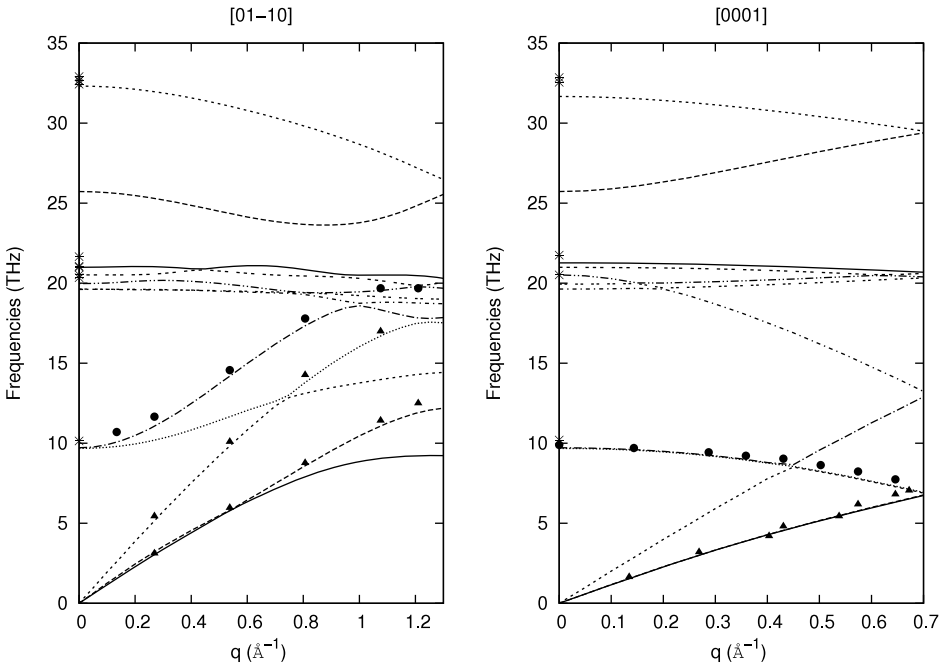

Figure 4. Dispersion plots along [01$\bar{1}$0] and [0001] to explicitly show the experimental data. The ▲ are for acoustic modes while the ● are for optic ones from the neutron scattering data. The stars are from the Raman scattering data.

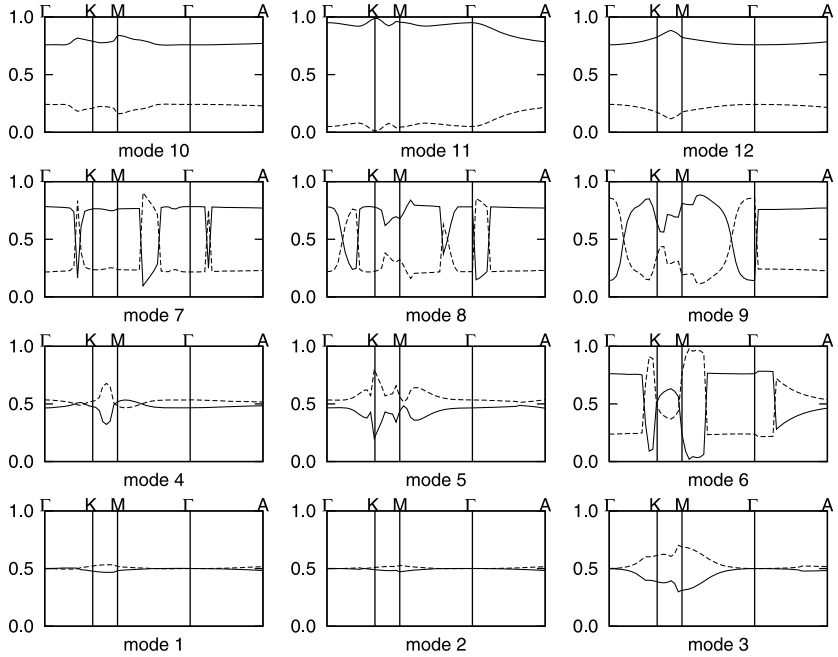

Figure 5. Squared vibrational amplitudes along some high symmetry directions to show the contribution from both the sublattices to various phonon modes. The solid lines are for beryllium and dashed ones for oxygen.

In several other insulators like ZnO, GaAs etc the DFPT and polarization method both based on DFT is found to deviate (mostly overestimate) from the experimental value of electronic dielectric constant ε_∞ [31]. In our calculations, the average value of ε_∞ (3.07) for BeO is also found to overestimate the experimental value (2.99) by about 2.6% [32]. However the DFPT value from this work is found to have better agreement with the experimental value as compared to the polarization method ($\varepsilon_\infty = 3.15$) [31]. As for the effective charges the present *ab initio* calculation gives the effective charge for beryllium and oxygen to be $Z^*_{\mathrm{Be}} = 1.82e$ and $Z^*_{\mathrm{O}} = -1.84e$ in close agreement with the experimental value of $|Z^*| = 1.85e$ [32].

4.5. Elastic constants

The distinct elastic constants for the wurtzite structure are C_{11}, C_{12}, C_{13}, C_{33}, C_{44} and C_{66} out of which only the first

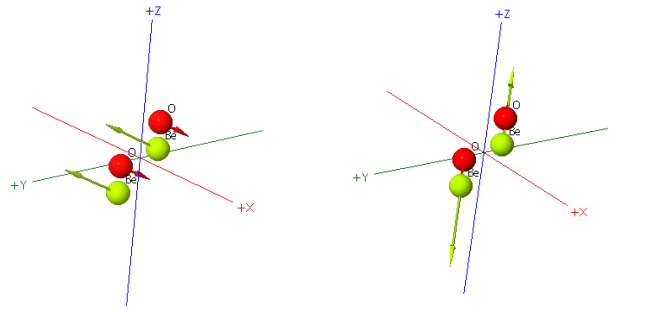

(a) mode : E_{1L} freq: 31.96[a], 32.91[b], 32.85[c]

(b) mode : A_{1L} freq: 25.72[a], 32.43[b], 32.55[c]

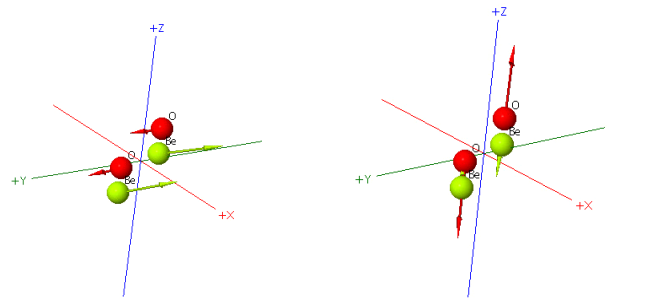

(c) mode : E_{1T} freq: 21.26[a], 21.66[b], 21.75[c]

(d) mode : A_{1T} freq: 20.52[a], 20.34[b], 20.52[c]

Figure 6. Atomic displacement patterns for split E_1 and A_1 modes along with their frequencies. Frequencies are in units of THz. This work[a], Arguello *et al* [30][b], Loh [10][c].

five are independent. C_{66} can be derived from C_{11} and C_{12} for systems with hexagonal symmetry. We use the following relations derived for hexagonal symmetry [33] to compute the various elastic constants from the slopes of the transverse and longitudinal acoustic branches for phonons propagating along Γ–A and Γ–M in the long wavelength limit.

Along Γ–A i.e. phonons propagating along the symmetry axis,

$$C_{33} = \rho(v_L)^2$$

$$C_{44} = \rho(v_T)^2.$$

Along Γ–M i.e. phonons propagating in the basal plane

$$C_{11} = \rho(v_L)^2$$

$$C_{66} = \tfrac{1}{2}(C_{11} - C_{12}) = \rho\,(v_{T1})^2$$

$$C_{44} = \rho(v_{T2})^2.$$

Here ρ is the mass density and v's are the sound velocities i.e. slopes of acoustic branches. In systems where the equilibrium value of c/a is close to the ideal value $\sqrt{(8/3)}$, we have $C_{13} + C_{33} \approx C_{11} + C_{12}$ [34] and in such a situation the hexagonal bulk modulus takes the form

$$B \approx \frac{2C_{13} + C_{33}}{3}.$$

Table 4. Elastic constants (in GPa) calculated from the phonon dispersion relation. The bulk modulus B (GPa) is calculated from the elastic constants.

Method	C_{11}	C_{12}	C_{13}	C_{33}	C_{44}	C_{66}	B
Phonon dispersion[a]	424.7	125.3	75.8	474.2	159.4	149.7	206.8
USP-GGA[b]	439.1	105.0	72.0	463.0	142.1	167.0	204.0
Ultrasonic[c]	461.0	126.5	88.5	491.6	147.7	167.0	224.0
Ultrasonic[d]	470.0	168.0	119.0	494.0	153.0	152.0	244.0
Debye–Waller[e]	468.0	130.0	120.0	497.0	148.0	169.0	240.0
Debye–Waller[f]	460.0	125.0	82.0	490.0	145.0	167.0	222.0

[a] This work.
[b] Ultrasoft pseudopotential based on GGA [35].
[c] Experiment with ultrasonic wave [36].
[d] Experiment with ultrasonic wave [37].
[e] X-ray Debye–Waller factor (extrapolated to 0 K) [38].
[f] X-ray Debye–Waller factor (data at room temperature) [38].

Since the equilibrium value of c/a in our system is 1.637, which is very close to the ideal value, we use the above approximations to compute C_{13} and B.

The results are shown in table 4. Here we compare our results with some available data from both theory and experiment. We see that the diagonal elements C_{11} and C_{33} and off-diagonal element C_{13} along with the bulk modulus from our USPP-GGA calculations have pretty good agreement (a maximum deviation of 5%) with the earlier USPP-GGA results [35]. The other elements have higher deviations ranging from 10% to 19%. This difference between the present USPP-GGA results and the earlier ones can be attributed, firstly to the difference in exchange correlation functionals used, and secondly to the approaches in calculating them. We have used the exchange correlation functional PW91 while the earlier work was done with PBE functional. On the other hand the existing results were derived from the stress–strain relationship by optimizing one against the other, while we have derived them entirely using the dispersion relations for the acoustic modes. As for the experimental results, they are pretty scattered amongst themselves for some coefficients and this therefore raises the question of reliability. However on average we have some 4.5%–14% deviations from the experimental values. C_{12} which had maximum deviation from the existing USPP-GGA result has excellent agreement with some of the experimental values (within 1%).

Therefore, our calculated elastic constants have reasonably good agreement with the existing theoretical and experimental results, implying the accuracy of our phonon calculations. This accuracy is desirable when one attempts to precisely find out the transition pressure where the system phase transforms structurally. As we had mentioned in the introduction, there is a controversy regarding the correct range of pressure where the structural transformation takes place in this compound. To resolve the issue of the discrepancy regarding the pressure range where the structural transition in this material takes place by investigating the role of vibrational contributions it is necessary that the phonons calculated under ambient conditions are accurate enough. Elastic constants are the ideal candidates to confirm this accuracy test as they are quite sensitive to any deformation.

5. Conclusions

From the present work, we draw the following conclusions regarding our results as well as the analysis of the underlying mechanism. Firstly the present *ab initio* results for the phonon dispersion relation in the ground state has very good agreement with the available INS data. However the frequency for the A_{1L} mode at the Γ-point has substantial disagreement with the Raman scattering data. But again our value is close to the one estimated from the projected beryllium oxide dispersion relation. Therefore a careful probing of the higher modes, both from theory as well as from experiment, is required. Secondly it has been noticed that in BeO, the split band behaviour in the phonon DOS is typical of the particular space group to which it belongs, while the feature that there exists a peak goes with some materials from the same oxide family. This means that in BeO the phonon dispersion and hence the phonon density of states characterizes the structural symmetry as well as the electronic configuration of the system. A mode by mode analysis of the contributions to the normal modes by various atoms has helped us to figure out that the modes around which the peak appears in the phonon DOS has fluctuating amplitudes of vibration across the Brillouin zone both from Be and O. Finally in order to test the accuracy of our phonon calculations we have computed the elastic constants of BeO from the slopes of acoustic modes and found that our values have reasonably good agreement with the available theoretical and experimental data. Since the long term motivation of this work is to study the pressure-induced phase transition in this oxide, the study of elastic constants from phonons is of particular importance. It will help us to understand the softening of elastic modes near the transition point at a particular pressure.

As to conclude, this complete understanding of the features in the phonon spectrum in the ground state and the derived properties would help us in doing calculations at elevated pressures to estimate the vibrational contributions and to understand the microscopic mechanism of phase stability in wurtzite–BeO.

Acknowledgments

MBS acknowledges the support from DST, Government of India for funding through the project No. SR/FTP/PS-39/2006 and is grateful to IIT Guwahati for making the physics department computational facilities available. We would like to thank Professor Eyvaz Esaev, Theoretical Physics Department, Moscow State Institute of Steel and Alloys, Russia for providing us with the code for computing partial phonon density of states. We are also grateful to Eva Moedlhammer, Library/GESS, IAEA's laboratories Seibersdorf for providing us with the report containing some experimental data.

References

[1] Bragg W L 1920 *Phil. Mag.* **39** 647
[2] Chang K J and Cohen M L 1984 *Solid State Commun.* **50** 487
[3] Camp P E V and Doren V E V 1996 *J. Phys.: Condens. Matter* **8** 3385
[4] Boettger J C and Wills J M 1996 *Phys. Rev.* B **54** 8965
[5] Park C, Lee S, Ko Y and Chang K J 1999 *Phys. Rev.* B **59** 13501
[6] Yingxiang C, Songtao W, Rui X and Jie Y 2006 *Phys. Rev.* B **73** 184104
[7] Young J A 1966 *Reactor Physics in the Resonance and Thermal regions, I* (Cambridge, MA: MIT Press)
[8] Ostheller G L, Schmunk R E, Brugger R M and Kearney R J 1968 *Neutron Inelastic Scattering* (Vienna: IAEA) p 315
[9] Brugger R M, Strong K A and Carpenter J M 1966 *J. Phys. Chem. Solids* **28** 249
[10] Loh E 1968 *Phys. Rev.* **166** 673
[11] Baroni S, Giannozzi P and Testa A 1987 *Phys. Rev. Lett.* **58** 1861
[12] Baroni S, Gironcoli S D, Corso A D and Giannozzi P 2001 *Rev. Mod. Phys.* **73** 515
[13] Hohenburg P and Kohn W 1964 *Phys. Rev.* B **136** 864
[14] Kohn W and Sham L J 1965 *Phys. Rev.* **140** A1133
[15] Jon R O and Gunnarson O 1989 *Rev. Mod. Phys.* **61** 689
[16] QUANTUM-ESPRESSO is a community project for high-quality quantum-simulation software based on density functional theory and coordinated by Paolo Gianozzi, See http://www.quantum-espresso.org and http://www.pwscf.org
[17] Vanderbilt D 1990 *Phys. Rev.* B **41** 7892
[18] Laasonen K, Pasquarello A, Car R, Lee C and Vanderbilt D 1993 *Phys. Rev.* B **47** 10142
[19] See http://www.physics.rutgers.edu/~dhv/uspp
[20] Louie S G, Froyen S and Cohen M L 1982 *Phys. Rev.* B **26** 1738
[21] We used the pseudopotentials O.pw91_n.UPF from http://www.quantum-espresso.orgdistribution
[22] Pardew J P and Wang Y 1992 *Phys. Rev.* B **45** 13244
[23] Monkhorst H J and Pack J D 1976 *Phys. Rev.* B **13** 5188
[24] Wyckoff R W G 1963 *Crystal Structures* vol 1 (New York: Interscience)
[25] Sachin V A, Bolorizadeh M A, Kheifets A S and Ford M J 2003 *J. Phys.: Condens. Matter* **15** 3567
[26] Nakamura S N and Chichibu S F 2000 *Introduction to Nitride Semiconductor Blue Lasers and Light Emitting Diodes* (Boca Raton, FL: CRC Press)
[27] Davydov V Y, Kitaev Y E, Goncharuk I N, Smirnov A N, Graul J, Semchinova O, Uffmann D, Smirnov M B, Mirgorodsky A P and Evarestov R A 1998 *Phys. Rev.* B **58** 12899
[28] Schutt O, Pavone P, Windl W, Karch K and Strauch D 1994 *Phys. Rev.* B **50** 3746
[29] Serrano J, Romero A H, Manjon F J, Lauck R, Cardona M and Rubio A 2004 *Phys. Rev.* B **69** 094306
[30] Arguello C A, Rousseau D L and Porto S P S 1968 *Phys. Rev.* **181** 1351
[31] Bernardini F and Fiorentini V 1998 Electronic dielectric constants of insulators by the polarization method *Preprint* cond-mat/9806045
[32] Posternak M, Baldereschi A and Catellani A 1990 *Phys. Rev. Lett.* **64** 1777
[33] Wanner R and Meyer H 1973 *J. Low Temp. Phys.* **11** 715
[34] Vitos L 2007 *Computational Quantum Mechanics for Materials Engineers: the EMTO Method and Applications* (Berlin: Springer) p 108
[35] Milman V and Warren M C 2001 *J. Phys.: Condens. Matter* **13** 241
[36] Cline C F, Dunegan H L and Henderson G W 1967 *J. Appl. Phys.* **38** 1944
[37] Bentle G G 1966 *J. Am. Ceram. Soc.* **49** 125
[38] Sirota N N, Kuzmina A M and Orlova N S 1990 *Dokl. Akad. Nauk SSSR* **314** 856